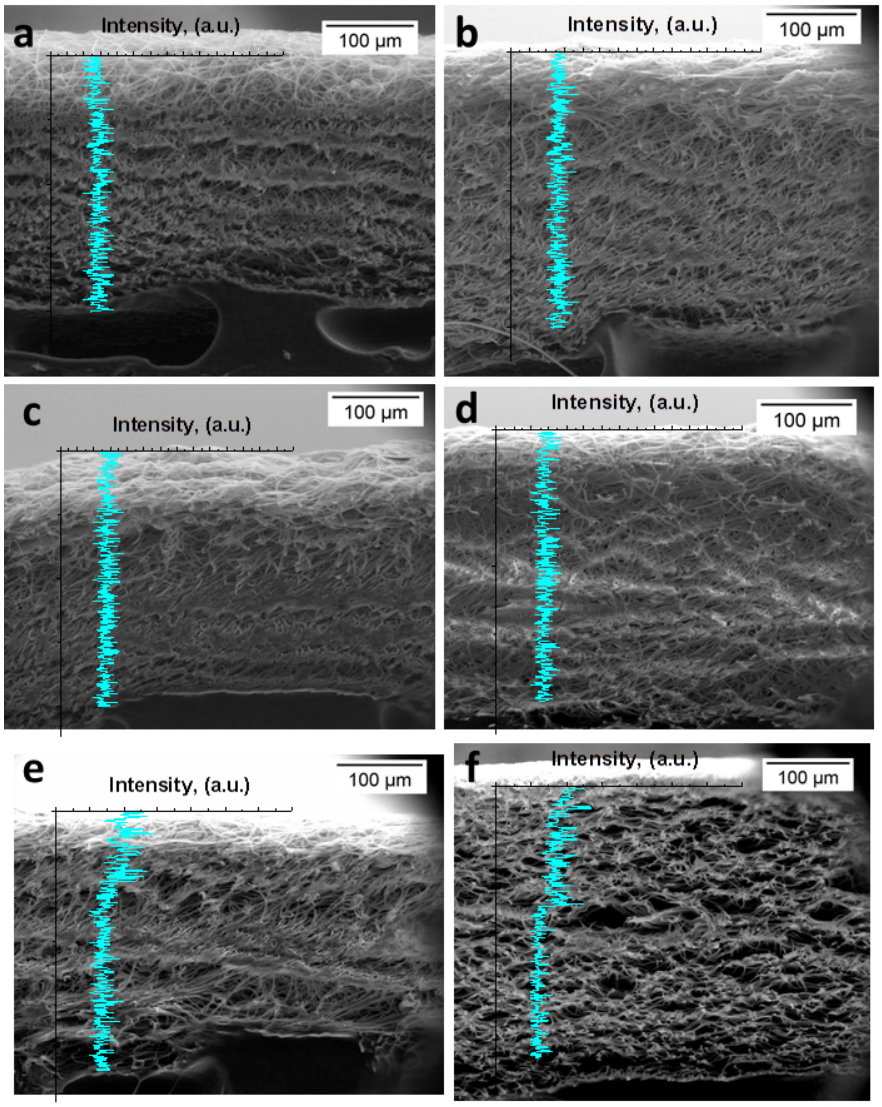

SEM images with overlap EDAX spectra of Ti of the elecrospun PCL scaffolds after the plasma treatment for the different time periods: (a) untreated scaffolds, scaffolds treated for 30 s (b), 60 s (c), 120 s (d), 240 s (e) and 480 s (f).

190x254mm (96 x 96 DPI)

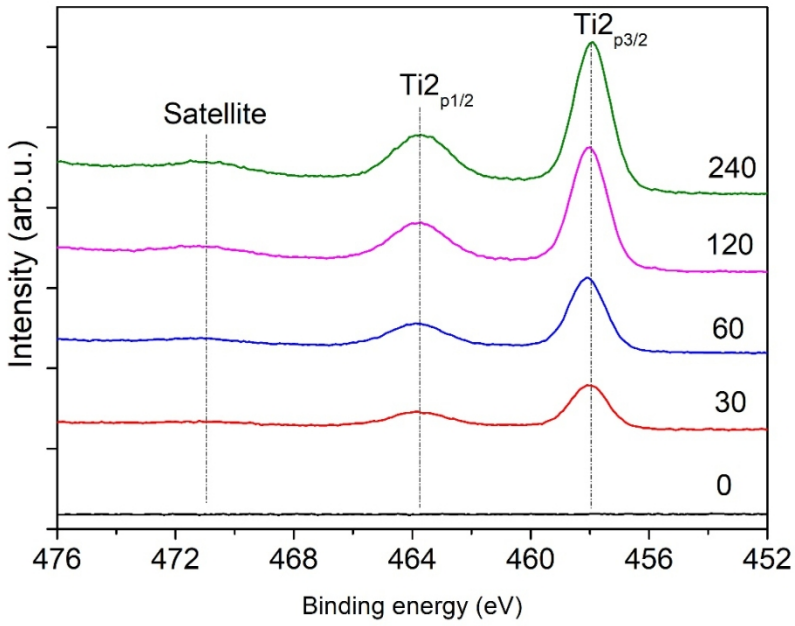

Ti2p core level spectra of the PCL scaffolds treated with plasma for: a) 30 s; b) 60 s; c) 120 s; d) 240 s.

148x103mm (220 x 220 DPI)

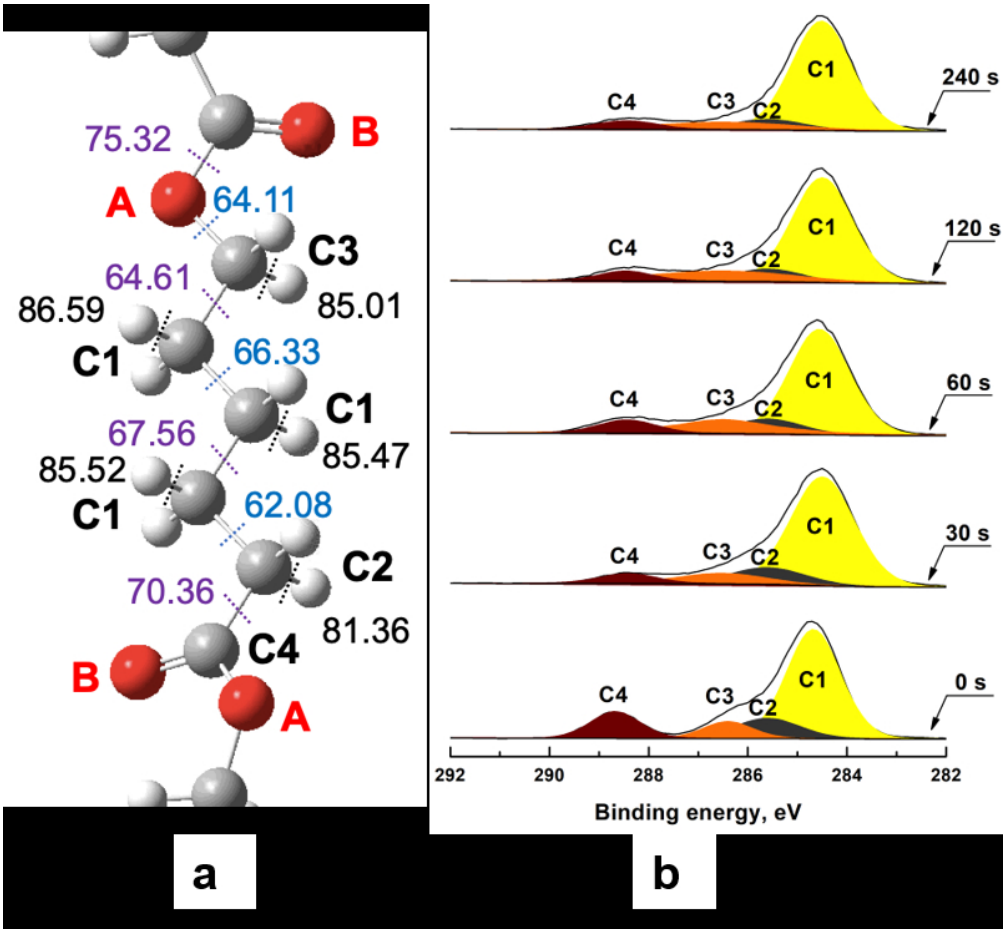

Representation of PCL chemical structure and the energies of the homolytic bond cleavage (kcal/mol) (a) and C1s (b), O1s (c) and N1s (d) core level spectra of the control PCL scaffolds (0 s) and PCL scaffolds treated with plasma for 30, 60, 120 and 240 s.

135x125mm (150 x 150 DPI)

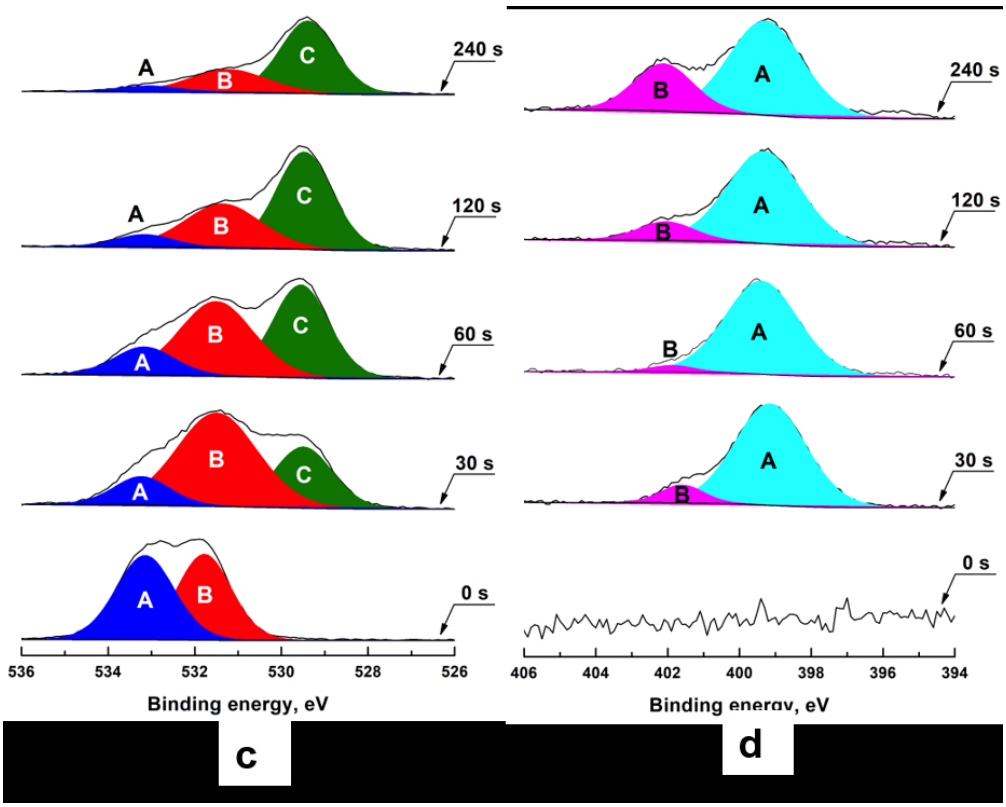

Representation of PCL chemical structure and the energies of the homolytic bond cleavage (kcal/mol) (a) and C1s (b), O1s (c) and N1s (d) core level spectra of the control PCL scaffolds (0 s) and PCL scaffolds treated with plasma for 30, 60, 120 and 240 s.

156x125mm (150 x 150 DPI)

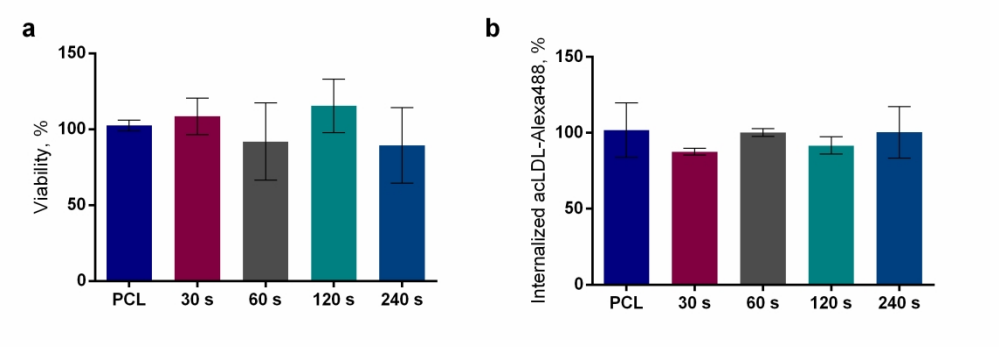

Viability (a) and endocytic activity (b) of human monocyte-derived macrophages cultured with unmodified and plasma treated PCL scaffolds for 6 days. Viability was evaluated using Alamar Blue assay. Endocytosis was studied by measuring uptake of acetylated low-density lipoprotein acLDL-Alexa488. The pooled data from three independent experiments are presented as mean ☐ SD. No significant differences were found ($p<0.0001$; one-way ANOVA with Tukey's correction).

250x87mm (300 x 300 DPI)

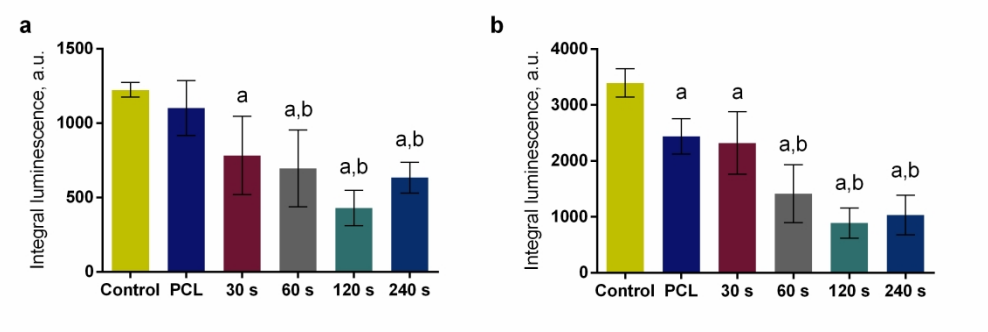

Effect of unmodified and plasma treated PCL scaffolds on spontaneous (a) and PMA-induced (100 nM) (b) ROS production by primary human monocytes. ROS was monitored for 1 h using Luminol chemiluminescence. The integral luminescence calculated over 1 h is shown. The data are presented as mean ☐ SD of 5 replicates from one experiment, and a representative experiment from three independent experiments is shown. Significant differences compared to the control (a) and PCL (b) are indicated ($p<0.0001$; one-way ANOVA with Tukey's correction).

277x93mm (300 x 300 DPI)

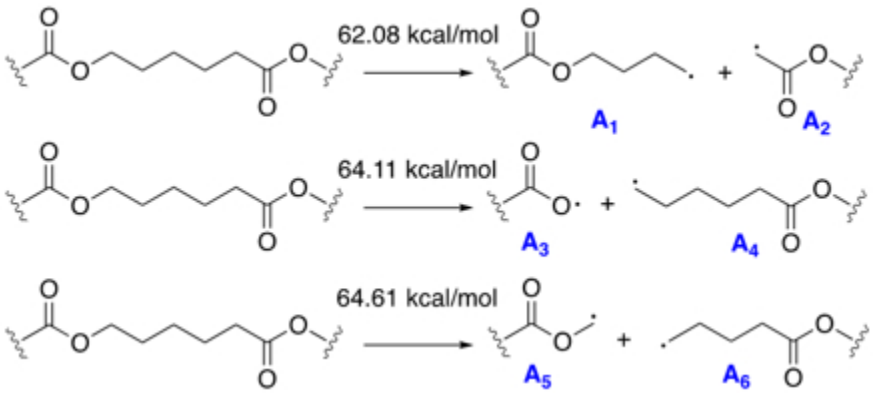

The thermodynamically favourable pathways of radical formation on the homolytic C-C bond cleavage in PCL.

73x33mm (150 x 150 DPI)

Modification of PCL scaffolds by reactive magnetron sputtering: a possibility for modulating macrophage responses

*Ksenia S. Stankevich[1,2], Valeriya L. Kudryavtseva[3,1], Evgeny N. Bolbasov[1,4], Evgeny V. Shesterikov[4,5], Irina V. Larionova[6,7], Yelena G. Shapovalova[6], Liubov V. Domracheva[6], Apollinariya A. Volokhova[1,6], Irina A. Kurzina[6], Yuri M. Zhukov[8], Anna B. Malashicheva[9,10], Julia G. Kzhyshkowska[6,11**], Sergei I. Tverdokhlebov[1*]*

1. *National Research Tomsk Polytechnic University, 30 Lenin Avenue, Tomsk, 634050, Russian Federation.*
2. *Montana State University, Culbertson Hall 100, Bozeman, Montana, USA.*
3. *Queen Mary University of London, Mile End Rd, Bethnal Green, London E1 4NS United Kingdom.*
4. *V.E. Zuev Institute of Atmospheric Optics SB RAS, 1 Academician Zuev square Tomsk, 634055, Russian Federation.*
5. *Tomsk State University of Control Systems and Radioelectronics, 40 Lenin Avenue Tomsk, 634050, Russian Federation.*
6. *Tomsk State University, 36 Lenin Avenue Tomsk, 634050, Russian Federation.*
7. *Cancer Research Institute, Tomsk National Research Medical Center, Russian Academy of Sciences, 9 Kooperativnii pereulok, Tomsk, 634050, Russian Federation.*
8. *Saint-Petersburg State University, 11/2 Lieutenant Schmidt emb., St. Petersburg, 199034 Russian Federation.*
9. *ITMO University, Institute of translational Medicine, 49 Kronverksky prospekt, Saint Petersburg, 197101, Russian Federation.*
10. *Federal Almazov Medical Research Centre, 2 Akkuratova street, St. Petersburg, 19734, Russian Federation.*

11. Institute of Transfusion Medicine and Immunology, Medical Faculty Mannheim, University of Heidelberg, Institute of Transfusion Medicine and Immunology, Medical Faculty Mannheim 13-17 Ludolf-Krehl-Straße, 68167 Mannheim, Germany.

‘

⁘**Corresponding Author**
E-mail: tverd@tpu.ru (S.T.)
E-mail: julia.kzhyshkowska@medma.uni-heidelberg.de (J.K)

KEYWORDS: *magnetron sputtering, poly (ε-caprolactone) scaffolds, DFT, immune response, macrophage*

ABSTRACT: Direct current (DC) reactive magnetron sputtering is as an efficient method for enhancing the biocompatibility of poly (ε-caprolactone) (PCL) scaffolds. However, PCL chemical bonding state, the composition of the deposited coating and their interaction with immune cells remains unknown. Herein, we demonstrated that DC reactive magnetron sputtering of the titanium target in a nitrogen atmosphere leads to the formation of nitrogen-containing moieties and the titanium dioxide coating on the scaffolds surface. We have provided the possible mechanism of PCL fragmentation and coating formation supported by XPS results and DFT calculations. Our preliminary biological studies suggest that DC reactive magnetron sputtering of titanium target could be an effective tool to control macrophage functional responses towards PCL scaffolds as it allows to inhibit respiratory burst while retaining cell viability and scavenging activity.

1. INTRODUCTION

During the last decades much attention has been drawn to the development of the tissue engineering scaffolds based on synthetic biodegradable polymers [1,2]. Poly (ε-caprolactone) (PCL) is a superior polymer for being considered as a biomaterial for a scaffold production due to adjustable biodegradability, lack of isomers and good physico-mechanical properties [3]. PCL-based tissue engineering scaffolds can be produced by a number of techniques [4] and be present in the form of films [5,6], 3D printed structures [7,8] and electrospun scaffolds [9]. Among them, electrospinning (ES) is the most promising and commonly used one [10–14]. An ability of fibrous PCL-based scaffolds fabricated by ES to mimic the structure of extracellular matrix (ECM) and their good mechanical performance [10] make them suitable for various biomedical applications [15].

Despite all the advantages and the fact that several PCL-based medical devices have been already approved by FDA to be used in human [16], the hydrophobicity of PCL and a lack of functional groups hinder the material interaction with surrounding cells and tissues [17]. Several approaches have been applied to improve electrospun PCL-based scaffolds properties including surface modification [18,19] and composite production [20–23]. Previously we have reported that polymer biodegradable scaffolds can be modified by reactive magnetron plasma that occurres under a working gas atmosphere during the sputtering of a solid target [24–26]. It was shown that direct current (DC) plasma magnetron sputtering is an effective tool to increase polymer biocompatibility and set specific surface properties by means of different plasma parameters and treatment conditions. Recently, we demonstrated the possibility of PCL-based scaffolds modification by DC reactive magnetron sputtering of the titanium target in a nitrogen atmosphere [19]. This promising technique allows for the deposition of thin titanium-nitrogen coatings on the surface of thermoplastic polymers with low melting points such as PCL. The modification at certain parameters improved the biocompatibility and hydrophilicity of the PCL-based scaffolds without affecting their physico-mechanical properties. However, the influence of the reactive plasma treatment at different regimes on the PCL chemical bonding state as well as the composition of the deposited coating remains unknown. Given that surface chemistry has a major impact on cell response to biomaterials [3], this issue requires in-depth studies.

Although the modified PCL-based scaffolds showed good biocompatibility towards endothelial cells [19], their interaction with immune cells have not been studied. The adverse immune reactions to the implanted material can lead to immediate negative outcomes such as

intense pain, inflammation or even rejection or delayed effects such as chronic inflammation [27,28]. In all cases, scaffold loses its function as supportive platform for tissue regeneration. Among the immune cells, macrophages play a key role in mediating immune response towards implanted materials orchestrating the inflammation and tissue remodeling stages [29–31]. The PCL-based scaffolds with titanium-nitrogen coating might have dual effect on macrophages. On the one hand, titanium and titanium dioxide are considered to be biocompatible, for example, it was shown that hydrophilic rough titanium surface induces anti-inflammatory macrophage activation [32,33]. On the other hand, titanium wear particles released from the scaffold surface might result in proinflammatory response [34,35]. Thus, it is crucial to study the immune reactions towards the PCL-based scaffolds modified by DC reactive magnetron sputtering of the titanium target in a nitrogen atmosphere.

The aim of the research is to investigate the influence of the DC plasma treatment at different regimes on the PCL chemical bonding state as well as the composition of the deposited coating and its effect on human macrophages.

2. MATERIALS AND METHODS

2.1 Scaffolds Production

The fibrous scaffolds were produced by electrospinning (ES) from an 8% solution of PCL (80,000 g/mol, Sigma-Aldrich, UK) in chloroform (Fisher, UK) using NANON-01A (MECC Co., Japan) equipment. The following technological parameters were applied: a flow rate of the polymer solution – 5 mL/h, a needle-to-collector distance – 190 mm, and a voltage – 20 kV. The thickness of obtained scaffolds – 280±23 μm.

2.2 DC Plasma Treatment

The produced PCL scaffolds were placed in a vacuum at 10^{-2} Pa for 10 h before the modification in order to remove the residual solvent. Scaffold modification was performed using the magnetron sputtering system described by us earlier [36] in a DC mode at the following parameters: the target material – chemically pure (99.99%) titanium (*Ti*); the atmosphere – dry 99.99% nitrogen (N_2), the power discharge – 40 W; the current – 0.2 A; the operating pressure in the chamber – 0.7 Pa; the distance between magnetron and the target – 40 mm; the magnetron area – 240 cm^2; and the modification times – 30, 60, 120, 240 and 480 s.

2.3 Scanning Electron Microscopy (SEM)

The images of the cross-section of the produced PCL scaffolds were obtained by SEM on an ESEM Quanta 400 FEG instrument (FEI, USA). Prior to the investigation, samples were coated

with a thin gold layer by the magnetron sputtering system (SC7640, Quorum Technologies Ltd., UK). The distribution of titanium concentration across the thickness of electrospun fibrous scaffolds was studied by EDS (Genesis 4000, EDAX). Three independent experiments were performed. In each experiment data were collected from at least 5 different areas.

2.4 X-Ray Photoelectron Spectroscopy (XPS)

XPS measurements were carried out with an Escalab 250Xi instrument (Thermo Fisher Scientific Inc., UK) equipped with a monochromatic AlKα radiation source (photon energy of 1486.6 eV). The spectra were obtained in constant-pass energy mode at 100 eV for the survey spectrum and 50 eV for the element core-level spectrum. The spot size of the X-ray beam was 650 μm, and the total energy resolution was around 0.55 eV. Studies were conducted at room temperature in an ultrahigh vacuum (with pressure of the order of 1×10^{-9} mbar; in the electron–ion compensation system, the Ar partial pressure was 1×10^{-7} mbar). The library of the reference XPS spectra, including the atomic registration sensitivity factors, was available in the Advantage Data System provided by the instrument manufacturer. The deconvolution o the peaks was performed using Avantage software (Thermo Fisher Scientific Inc., UK) set to Shirley background subtraction followed by peak fitting to Voigt functions with an 80% Gaussian and 20% Lorentzian character. Each XPS experiment included 2 replicates. The measurements were performed at least at 2 different locations for each replicate.

2.5 DFT studies

The theoretical calculations of neutral PCL and PCL radicals were performed using Kohn−Sham density functional theory (DFT) in Gaussian 16 (Revision C.01) software [37]. Model PCL chains consisting of five monomers were fully optimized using global-hybrid GGA functional B3LYP [38] that has been successfully used for similar systems before [39] and standard 6-311++G(2d,p) basis set. The stationary points were confirmed by harmonic frequency calculations.

2.6 Monocytes isolation and culture

Monocytes were isolated from the buffy coats of the healthy donors provided by the German Red Cross Blood Service Baden-Württemberg – Hessen and from Tomsk Regional Blood Center (Tomsk, Russia) as described previously [40]. German cohort of donors was used for endocytosis assay, Russian cohort – for viability assay and luminescence assay. Briefly, CD14 monocytes were purified by sequential Biocoll (Biochrom, Germany) and Percoll (Pharmacia, Germany) density gradient centrifugation with subsequent positive magnetic selection using CD14 microbeads (Miltenyi Biotec). Isolated monocytes were resuspended at a concentration of 10^6 cells/ml in *X-VIVO 10* serum free medium (Lonza, USA) supplemented with 1 ng/mL

m-CSF (Peprotech, Germany) and 10^{-8} M dexamethasone (Sigma-Aldrich, Germany). Control PCL scaffolds and PCL scaffolds treated with plasma for 30, 60, 120 and 240 s were cut in 1×1 cm square-shaped pieces and sterilized with ethylene oxide. Scaffolds were placed into the wells of 24-well plate; cells cultured without a material were used as a control. For each well 2 ml of cell suspension containing 2×10^6 monocytes were added on top of the scaffold and cultured for 6 days in CO_2 incubator at 37°C.

2.7 Cell viability assay

The effect of the fabricated scaffolds on macrophage viability on day 6 was studied using Alamar Blue assay (ThermoFisher, USA). To perform the analysis Alamar Blue was added in 1:10 proportion in culture medium followed by 3 h incubation at 37°C. Thereafter, supernatants were collected in a 96-well plate and the absorbance was monitored at 570 nm and 600 nm. Three independent experiments were performed, with each experiment containing 2 replicates. The viability was calculated as percentage relative to control.

2.8 Endocytosis

To study endocytic ability of macrophages after co-culture with the scaffolds, the uptake of acetylated low-density lipoprotein acLDL-Alexa488 (ThermoFisher, USA) was evaluated. On day 6 after the incubation, acLDL was added to the cells cultured on scaffolds at a concentration of 2 μg/mL for 30 min. The cells were then detached from the scaffold surface using 0.25% Trypsin-EDTA solution and washed three times with PBS (Gibco, USA). Quantitative analysis of fluorescent ligand internalization was performed using flow cytometry (BD FACSCanto II, Germany). Three independent experiments were performed, with each experiment containing 2 replicates.

2.9 Reactive oxygen species (ROS) production

ROS production was measured by Luminol-based luminescence assay. Control PCL scaffolds and PCL scaffolds treated with plasma for 30, 60, 120 and 240 s were cut in 5 × 5 mm square-shaped pieces, sterilized with ethylene oxide and then placed into the wells of a 96-well plate. Prior to the cell addition, 100 μL of HBSS containing Ca^{2+} and Mg^{2+} without phenol red ($HBSS^+$) were added to each well. To evaluate the influence of the materials on spontaneous ROS production, freshly isolated human monocytes were resuspended at 10^6 cells/mL in $HBSS^+$ supplemented with 40 μM of Luminol and aliquoted (100 μL) into the wells on top of the scaffolds. To evaluate the influence of the materials on phorbol 12-myristate-13-acetate (PMA) induced ROS production, freshly isolated human monocytes were resuspended at 10^6 cells/mL in $HBSS^+$ supplemented with 40 μM of Luminol, aliquoted (100 μL) into the wells

on top of the scaffolds and immediately stimulated with 100 nM PMA. Monocytes incubated without scaffold were used as a negative control, whereas monocytes incubated without scaffold and stimulated with 100 nM PMA were used as positive control. Luminescence was monitored for 1 h with a 5-min reading interval using an Anthos Lucy 3 microplate reader (Anthos Labtec Instruments GmbH, Austria). The curve of light intensity (in relative luminescence units) was plotted against time, and the area under the curve was calculated as integral luminescence. Three independent experiments were performed, with each experiment containing 5 replicates.

2.10 Statistics

The data were analyzed with GraphPad Prism 8 software using the one-way ANOVA with Tukey's correction. The difference was considered significant at a significance level of $p<0.05$.

3. RESULTS AND DISCUSSION

SEM images with overlapped EDAX Titanium spectra of the cross-section of elecrospun PCL scaffolds are shown in **Figure. 1**.

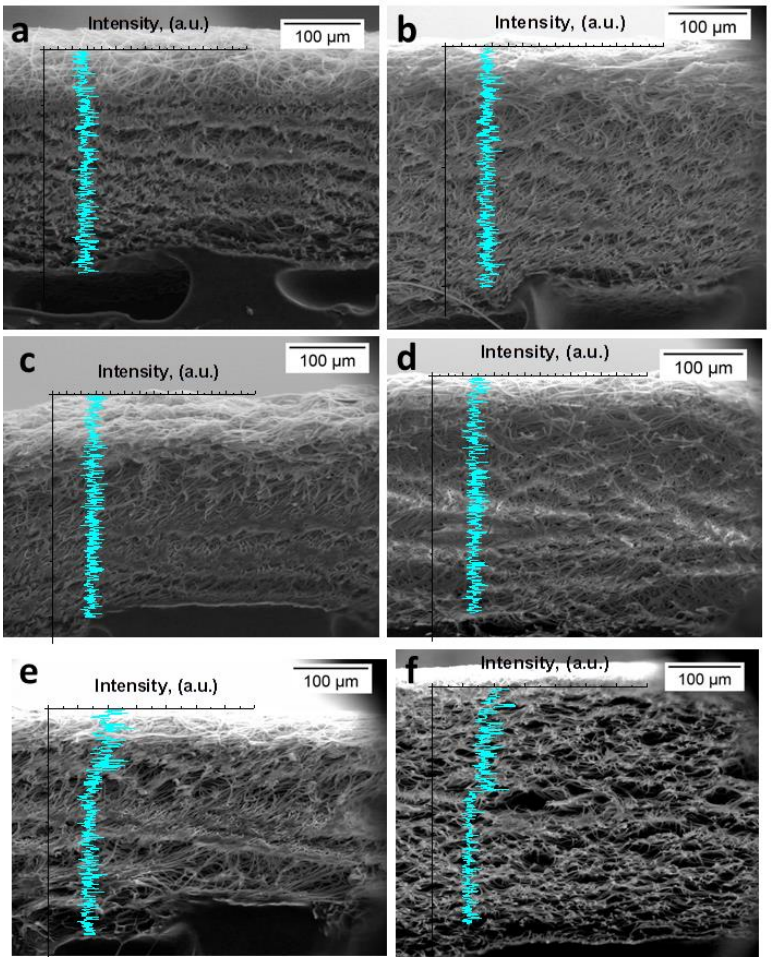

Figure. 1. SEM images with overlap EDAX spectra of *Ti* of the elecrospun PCL scaffolds after the plasma treatment for the different time periods: (a) untreated scaffolds, scaffolds treated for 30 s (b), 60 s (c), 120 s (d), 240 s (e) and 480 s (f).

The electrospun PCL scaffold consists of randomly intertwined cylindrical fibres with an average diameter of 3.1 ± 0.3 μm and pore sizes 22.3 ± 5.4 μm. The cross-sectional study of the scaffolds shows that the distribution of titanium concentration across the thickness of electrospun fibrous scaffolds is not homogeneous. This is evidenced by the intensity profile of the *Ti* K line in the direction from the surface to the inner volume of the sample. There is no noticeable *Ti* signal in samples treated for 30 – 120 s. In sample treated for 240 s *Ti* was located within a thickness of approximately 100 μm, when treatment time was increased up to 480 s *Ti* penetrated deeper into sample to a depth of approximately 150 μm.

It could be explained by two mechanisms: re-spraying of *Ti* and water/ions interaction. The depth of the ions penetration into the bulk of the sample as well as the efficiency of the coating re-spraying is proportional to the energy of the particles impacting the target. Thus, the *Ti* penetration to the scaffold bulk is determined by the voltage and current between the sputtering

target and cathode. Considering the fact that the discharge parameters were not changed during the experiment, the depth of *Ti* penetration into the inner volume of the scaffold increased due to re-spraying [36].

Moreover, *Ti* interaction with thin layer of absorbed water on the top of fibers and inside pores is very likely processes which end up in oxidation reaction of titanium and formation thin layer of TiO_2. When water molecules absorbed on the closest to target layer of fibers interacted with *Ti* ions, ions penetrate deeper in to the bulk of scaffold [41,42]. Due to considerable changes in composition in the bulk of the material which may lead to changes in physical properties sample treated for 480 s was excluded from further studies.

Table 1 shows an elemental composition of the surface of the control and modified PCL scaffolds determined by XPS. The control scaffold contains carbon and oxygen in a ratio typical for PCL [22]. After the plasma treatment titanium and nitrogen appear on the scaffold surface (**Table 1**). The atomic percentage of titanium on the PCL scaffold surface increases with an increase in the treatment time. It is in agreement with our previous studies, where an increase in the titanium amount on the material surface was observed by EDS analysis [43]. Considering the Ti2p spectrum of the plasma-treated PCL film, where three peaks corresponding to TiO_2 can be found, namely, $Ti2_{p1/2}$ at 464.2 eV, $Ti2_{p3/2}$ at 458.3 eV, and satellite peak at 471.5 eV, we can conclude that TiO_2 coating is deposited during the DC plasma treatment **(Figure. 2**). The formation of TiO_2 is also confirmed by O1s core level spectra of the plasma treated scaffolds, where an additional low-energy component corresponding to Ti-O bond appears (**Figure. 3 c)**. This component increases with an increase in the plasma treatment time (**Table 2**, **Figure. 3 c**). Thus, the XPS results support the mechanisms of Ti penetration into the bulk of the scaffold described above. The atomic percentage of oxygen on the scaffold surface also increases, whereas the atomic percentage of nitrogen does not change significantly over the treatment time. No Ti-N components are observed in the Ti2p or N1s spectra (**Figure. 2, Figure. 3 d**).

Table 1. Elemental composition of the surface of the control and modified PCL scaffolds determined by XPS.

Sample	C [at.%]	O [at.%]	N [at.%]	Ti [at.%]	Atomic ratio	
					C/O	Ti/N
Control	77.3	22.7	-	-	3.41	-

30	67.3	22.1	6.2	4.4	3.04	0.72
60	57.7	28.6	5.9	7.8	2.02	1.33
120	50.1	32.2	5.9	11.8	1.55	2.00
240	44.8	34.6	5.9	14.7	1.29	2.46

Thus, despite of the fact that plasma treatment was conducted in dry 99.99% N_2, the deposition of TiO_2 instead of TiN is observed at all the studied parameters. As we reported earlier, the remaining water on the scaffold surface may account for this process [44]. Since the formation of TiO_2 is thermodynamically favoured over TiN [44], the ions from the sputtering target react first with water giving TiO_2.

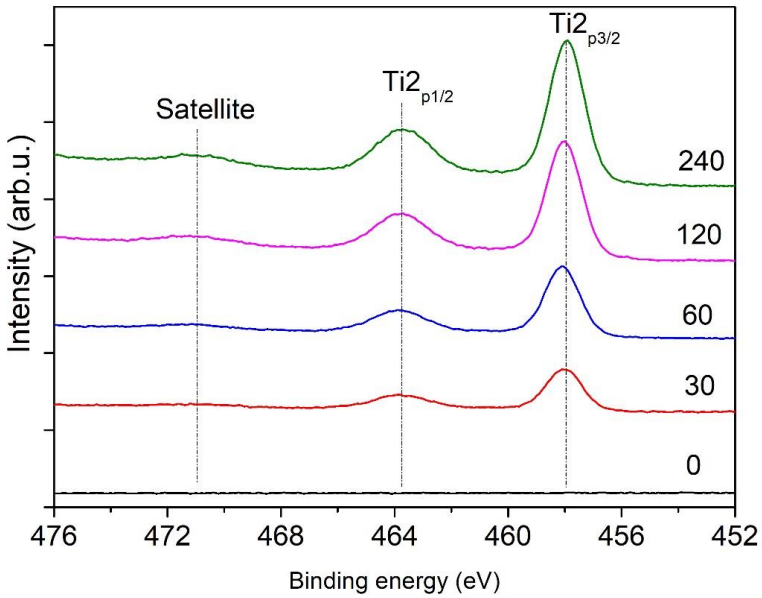

Figure. 2. Ti2p core level spectra of the PCL scaffolds treated with plasma for: a) 30 s; b) 60 s; c) 120 s; d) 240 s.

Table 2. Relative area corresponding to the chemical bonds on the surface of the investigated PCL scaffolds obtained after O1s core level spectra deconvolution.

Sample	**Relative area corresponding to different chemical bonds on the PCL surface, %**		
	C-O-C/C-OH (A), %	**O=C (B), %**	**Ti-O (C), %**
Control	49	51	-
30	60	12	28

60	44	14	42
120	36	7	57
240	28	5	67

Table 3 shows the relative area corresponding to the chemical bonds on the surface of the investigated PCL scaffolds obtained after C1s and N1s core level spectra deconvolution (**Figure. 3**). An initial relative ratio of the C1-C4 components in the C1s spectrum of the control PCL scaffolds correlates with the published data [22,45,46] except an increased C1 component due to the carbon contamination. Plasma treatment for 30 s altered the shape of C1s peak, increasing C1 component and decreasing C4 component. The further increase in the treatment time resulted in decrease in C2 and increase in C3 components (**Figure. 3 b**).

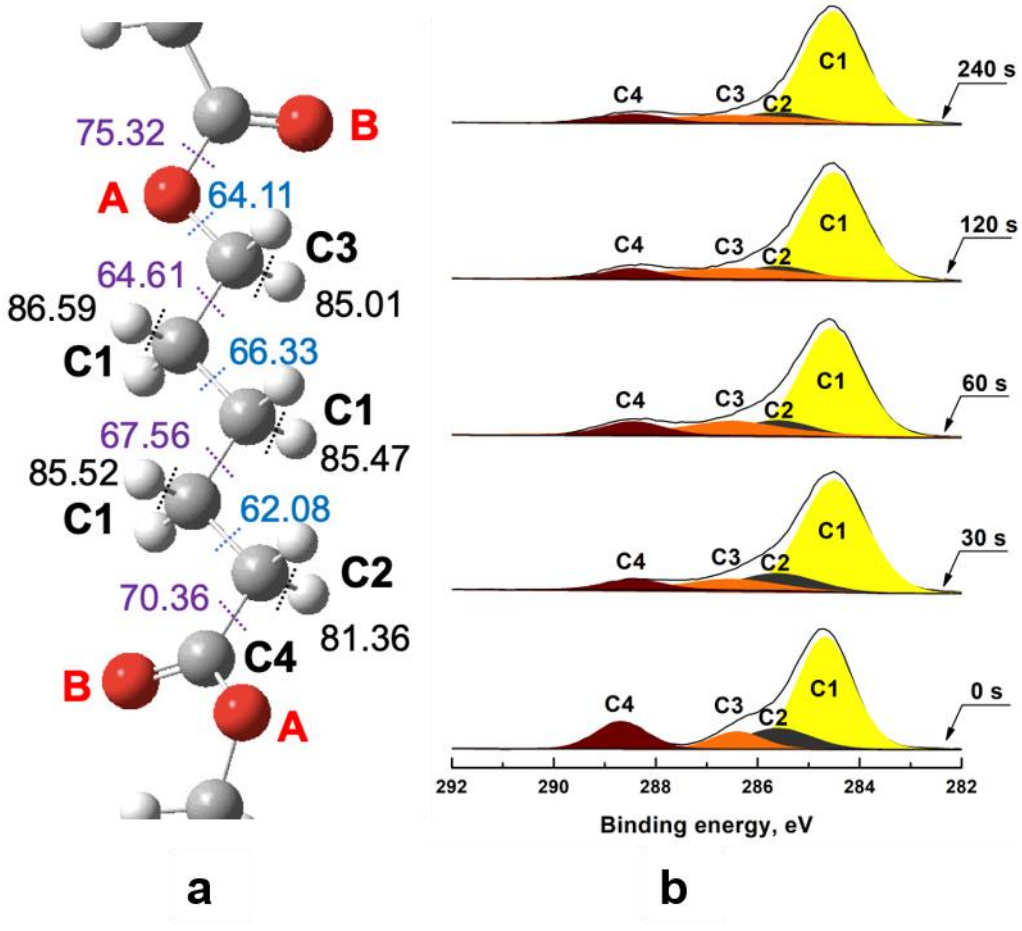

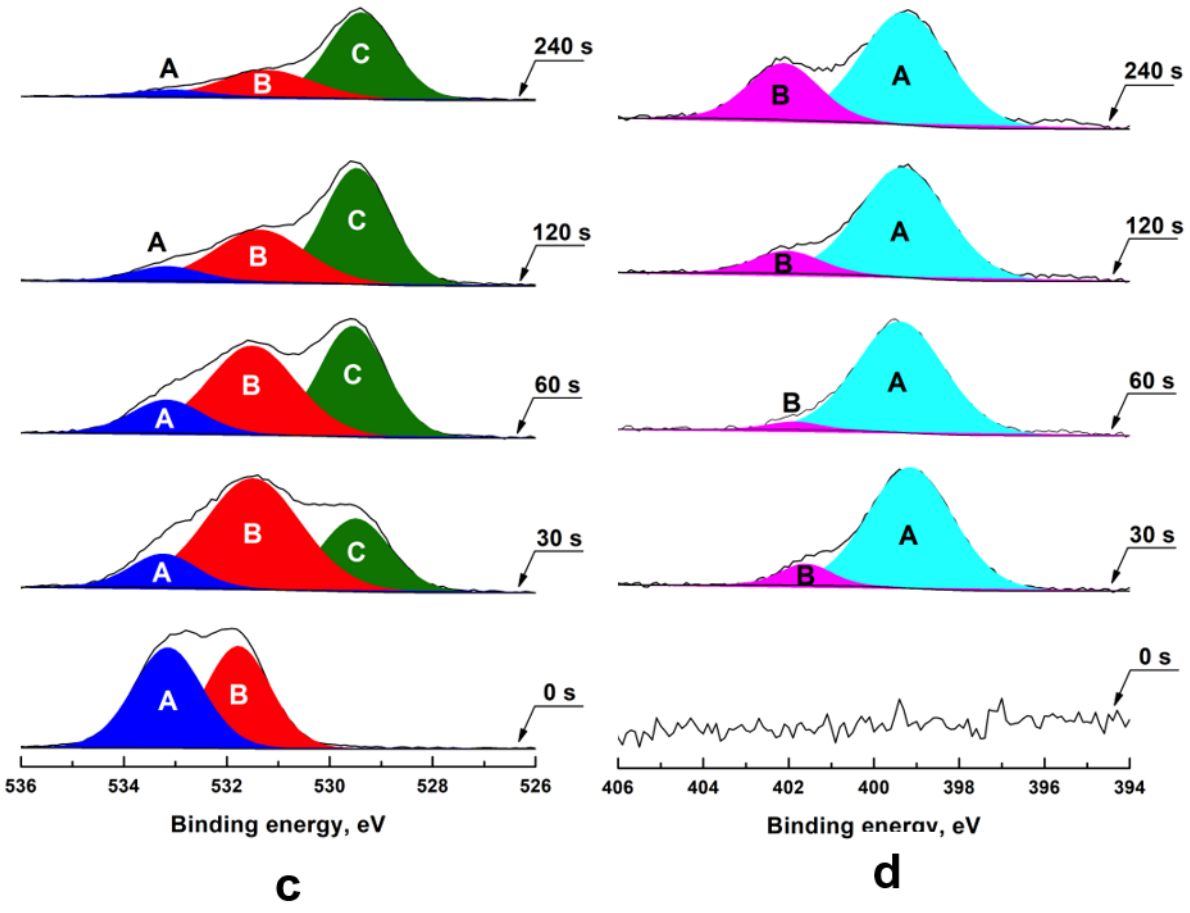

Figure. 3. Representation of PCL chemical structure and the energies of the homolytic bond cleavage (kcal/mol) (a) and C1s (b), O1s (c) and N1s (d) core level spectra of the control PCL scaffolds (0 s) and PCL scaffolds treated with plasma for 30, 60, 120 and 240 s.

The mechanism of the coating deposition on PCL-based scaffolds surface is probably similar to one described for polylactic acid [25]. First, N^{2+} ions from plasma attack the PCL surface with the formation of N· radicals. The simultaneous scissions of C-C, C-H and C-O bonds in PCL could result in generation of various radicals. The energy available during the plasma treatment largely exceeds the amount required to cleave any bond in PCL. However, the process of bond scission is not random since formed radicals have different stability (**Figure. 3 a**).

The predict the radicals that are more likely to appear on the PCL surface, the DFT calculations at the B3LYP/6-311++G(2d,p) level of theory were performed. According to the results, the least amount of energy (62.08 kcal/mol) is required for the cleavage of C-C bond in PCL chain according to the top reaction shown in **Scheme 1**. It can be explained by the

relative stability of radical A_2 stipulated by conjugation between CH_2· radical center and the neighbouring carboxy group.

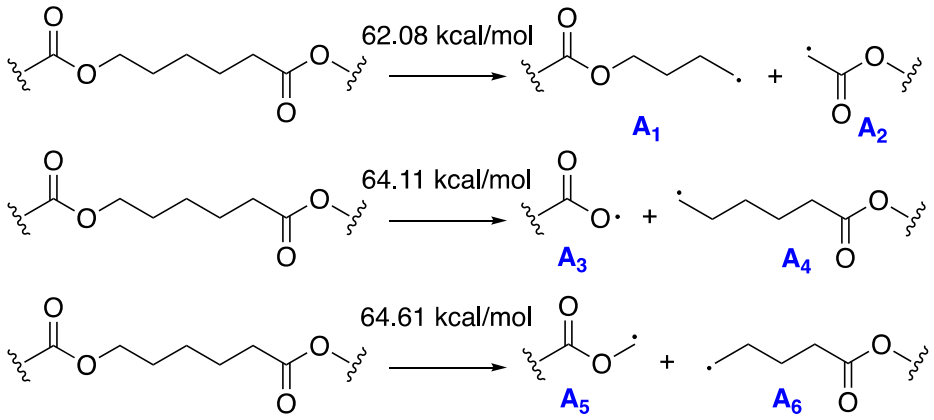

Scheme 1. The thermodynamically favourable pathways of radical formation on the homolytic C-C bond cleavage in PCL.

The energies required for the generation of other radicals from PCL are shown in **Figure. 3 a**. The cleavage of C-O bond with the formation of peroxy radical A_3 (64.11 kcal/mol) is the second possible pathway according to the calculation results (**Figure. 3 a**). The least thermodynamically favourable pathway is proton abstraction (**Figure. 3 a**).

The cleavage of C-C bond with the formation of radicals A_1 and A_2 and subsequent incorporation of oxygen into PCL chain as [–C–O–C–] or [–(C–OH)–] moieties would result in increased C3 and decreased C2 component as observed by XPS (**Table 3, Figure. 3 b**). The A_3 radical may undergo rearrangement followed by the elimination of CO_2. It would result in the decreased C4 component corresponding to C=O bond and increased C1 component.

Table 3. Relative area corresponding to the chemical bonds on the surface of the investigated PCL scaffolds obtained after C1s and N1s core level spectra deconvolution.

Sample	**Relative area corresponding to different chemical bonds in PCL, %**					
	Carbon				**Nitrogen**	
	C1	**C2**	**C3**	**C4**	**NH_2 and/or H_2NCO**	**NH_3+**
BE (eV)	285.0 ± 0.2	285.6 ± 0.2	286.5 ± 0.2	289.1 ± 0.2	399.9 ± 0.2	402.5 ± 0.2
PCL lit. [22]	52	17	17	14	-	-

Control	63	14	10	13	-	-
30	72	13	9	6	90	10
60	65	11	16	8	96	4
120	69	9	16	6	87	13
240	75	8	11	6	71	29

As can be seen from N1s spectra deconvolution after the plasma treatment (**Figure. 3 d)**, two components corresponding to amine and/or amide moieties (A, 399.6 eV) and protonated/hydrogen bonded amine groups (B, 402.3 eV) [47] appear. These functional groups can be formed as a result of the reaction between the PCL radicals (**Scheme 1**) and N· radical. The amide moiety could appear due to recombination of N· radicals and radicals generated after homolytic cleavage of C-O bond in carboxy group or C-C bond in C-COOH fragment. However, the formation of these species is less thermodynamically favourable - 75.32 kcal/mol and 70.36 kcal/mol, respectively. The relative ratio between the components A and B changes with an increase in plasma treatment time (**Figure. 3 d)**. It is observed that component B increases, most likely indicating the protonation/ hydrogen bonding of amino groups.

Overall, the XPS study shows that after the DC plasma treatment results in formation of nitrogen-containing moieties and the titanium dioxide coating on the PCL scaffolds surface. The functionalization of surface explains enhanced wettability and biocompatibility, observed by us earlier [44].

To investigate the effect of the deposited coating on immune cells, primary human CD14+ monocytes were isolated and cultured on modified scaffolds. First, we evaluated the effect of the fabricated materials on cell viability (**Figure. 4 a**). The results demonstrated that the deposited coatings are not toxic towards human monocyte-derived macrophages during 6-day culture period as cell viability did not differ significantly from the control PCL scaffolds.

We further studied the endocytic function of the macrophages cultured on scaffold surface via evaluation of acLDL-Alexa488 uptake (**Figure. 4 b**). We have found that after the co-culture with the scaffolds, monocyte-derived macrophages retain their endocytic ability indicating that they preserve scavenging function.

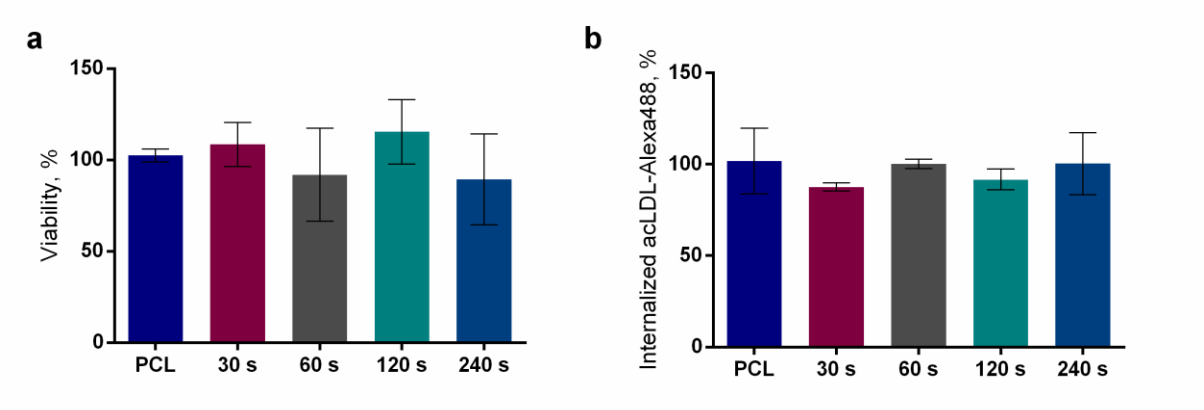

Figure. 4. Viability (a) and endocytic activity (b) of human monocyte-derived macrophages cultured with unmodified and plasma treated PCL scaffolds for 6 days. Viability was evaluated using Alamar Blue assay. Endocytosis was studied by measuring uptake of acetylated low-density lipoprotein acLDL-Alexa488. The pooled data from three independent experiments are presented as mean ± SD. No significant differences were found (p<0.0001; one-way ANOVA with Tukey's correction).

To evaluate monocyte proinflammatory response, we studied the effect of the scaffolds on spontaneous and PMA-induced ROS production (**Figure. 5**). Our results showed that while untreated PCL scaffolds had no inhibitory effect on spontaneous respiratory burst, scaffolds treated with plasma for more than 30 s significantly decreased ROS production (**Figure. 5 a**). In case of PMA-induced ROS production, untreated PCL scaffolds and scaffolds treated for 30 s slightly lowered ROS levels, whereas scaffolds treated for 60, 120 and 240 s had a pronounced inhibitory effect on respiratory burst (**Figure. 5 b**).

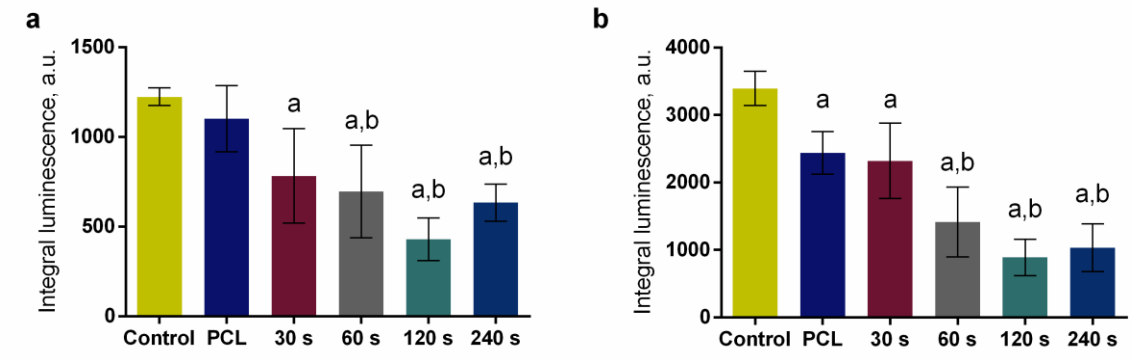

Figure. 5. Effect of unmodified and plasma treated PCL scaffolds on spontaneous (a) and PMA-induced (100 nM) (b) ROS production by primary human monocytes. ROS was monitored for 1 h using Luminol chemiluminescence. The integral luminescence calculated

over 1 h is shown. The data are presented as mean ± SD of 5 replicates from one experiment, and a representative experiment from three independent experiments is shown. Significant differences compared to the control (a) and PCL (b) are indicated (p<0.0001; one-way ANOVA with Tukey's correction).

The effect of the modified scaffolds on monocyte functional responses can be explained by physico-chemical and morphological properties of the materials. Surface wettability is an important factor that influences monocyte reaction [33]. As was shown by SEM/EDAX and XPS studies, one of the main components of the coating formed is TiO_2. It was previously reported that monocytes adhere well to Ti surface and demonstrate Ti-enhanced survival [48]. Similarly, we found modified materials to support macrophage viability over the cell culture period (6 days). Additionally, a hydrophilic TiO_2 along with nitrogen-containing moieties enhances hydrophilicity of the scaffold surface. Indeed, we found that an increase in the plasma treatment time from 0 to 240 s leads to a decrease in water contact angle from 123.0 ± 2.6 to 65.3 ± 2.9° [44]. It was reported that hydrophilic rough TiO_2 surfaces promote anti-inflammatory and pro-healing activity of macrophages [32,33]. Our study also demonstrates that with an increase in the plasma treatment time both spontaneous and PMA-induced ROS production by monocytes in response to material presence decreases. In addition, macrophages retain scavenging activity.

The other important factor affecting monocyte reaction is surface topography: electrospun PCL scaffolds might elicit different macrophage responses depending on mean fiber diameter. In particular, RAW264.7 macrophages cultured on electrospun PCL scaffolds with a fiber diameter of 116±30 nm had up-regulated mRNA expression of IL-6 and TNFα, whereas on protein level only elevated secretion of TNF-α was found [49]. The mRNA up-regulation of IL-6, TNF-α and MIF-1 in response to electrospun PCL scaffolds with a fiber diameter of 0.69±0.54 μm was also observed by authors in [50]. On the other hand, RAW264.7 macrophages cultured on PCL-based scaffolds with a mean fiber diameter of 5.59±0.67 μm had increased M2-associated gene expression including Argl and FiZZ1, which indicates that PCL-based scaffolds with thicker fibers might stimulate M2 polarization [51] . In current study PCL scaffolds had an average fiber diameter of 2.1±0.67 μm. Thus, a rather thick fibers along with surface chemistry could contribute to anti-inflammatory response.

Overall, our preliminary findings show that the plasma treatment improves scaffold biocompatibility towards macrophages mainly by altering surface chemistry of the materials. The deposited coating imparts anti-inflammatory properties as shown by ROS inhibition as

well as does not affect macrophage endocytic ability. However, the more comprehensive study of macrophage responses towards the modified scaffolds is further required. This study should address functional readouts of monocyte behavior (e.g. cytokine release, gene expression), monocyte phenotype and cell attachment to scaffolds.

CONCLUSIONS

Herein, we have investigated the influence of the DC reactive magnetron sputtering of titanium target in nitrogen atmosphere for various times on the PCL chemical bonding state. XPS analysis supported with DFT calculations showed that the plasma treatment results in scissions of C-C and C-O bonds in PCL leading to a formation of certain radicals. These radicals further interact with N· radicals from plasma or H_2O absorbed on the top of fibers and inside pores contributing to the appearance of amine and amide groups on PCL surface. Alternatively, they undergo rearrangement with the elimination of CO_2. Simultaneously, the formation of TiO_2 on the material surface is observed. An increase in the plasma treatment time results in deeper penetration of TiO_2 coating saturated with nitrogen-containing moieties to the bulk of the scaffold, which is proved by both EDAX and XPS. Our preliminary biological studies suggest that DC reactive magnetron sputtering of titanium target could be an effective tool to control human monocyte-derived macrophage functional responses towards PCL scaffolds. In particular, we have observed that with an increase in the plasma treatment time both spontaneous and PMA-induced ROS production by monocytes in response to material presence decreases. In addition, macrophages retain viability and scavenging activity.

NOTES

The authors declare no competing financial interest.

ACKNOWLEDGMENTS

This work was financially supported by Tomsk Polytechnic University Competitiveness Enhancement Program and Russian State Project “Science” (WSWW-2020-0011).

REFERENCES

(1) Ulery, B. D.; Nair, L. S.; Laurencin, C. T. Biomedical Applications of Biodegradable Polymers. *J. Polym. Sci. Part B Polym. Phys.* **2011**, *49* (12), 832–864. https://doi.org/10.1002/polb.22259.

(2) Nair, L. S.; Laurencin, C. T. Biodegradable Polymers as Biomaterials. *Prog. Polym. Sci.* **2007**, *32* (8–9), 762–798. https://doi.org/10.1016/j.progpolymsci.2007.05.017.

(3) Dave, K.; Gomes, V. G. Interactions at Scaffold Interfaces: Effect of Surface Chemistry, Structural Attributes and Bioaffinity. *Mater. Sci. Eng. C* **2019**, *105*, 110078. https://doi.org/10.1016/j.msec.2019.110078.

(4) Hutmacher, D. W. Scaffold Design and Fabrication Technologies for Engineering Tissues — State of the Art and Future Perspectives. *J. Biomater. Sci. Polym. Ed.* **2001**, *12* (1), 107–124. https://doi.org/10.1163/156856201744489.

(5) Woodard, L. N.; Grunlan, M. A. Hydrolytic Degradation of PCL–PLLA Semi-IPNs Exhibiting Rapid, Tunable Degradation. *ACS Biomater. Sci. Eng.* **2019**, *5* (2), 498–508. https://doi.org/10.1021/acsbiomaterials.8b01135.

(6) Asadpour, S.; Yeganeh, H.; Ai, J.; Kargozar, S.; Rashtbar, M.; Seifalian, A.; Ghanbari, H. Polyurethane-Polycaprolactone Blend Patches: Scaffold Characterization and Cardiomyoblast Adhesion, Proliferation, and Function. *ACS Biomater. Sci. Eng.* **2018**, *4* (12), 4299–4310. https://doi.org/10.1021/acsbiomaterials.8b00848.

(7) Kosik-Kozioł, A.; Graham, E.; Jaroszewicz, J.; Chlanda, A.; Kumar, P. T. S.; Ivanovski, S.; Święszkowski, W.; Vaquette, C. Surface Modification of 3D Printed Polycaprolactone Constructs via a Solvent Treatment: Impact on Physical and Osteogenic Properties. *ACS Biomater. Sci. Eng.* **2019**, *5* (1), 318–328. https://doi.org/10.1021/acsbiomaterials.8b01018.

(8) Garcia Garcia, A.; Hébraud, A.; Duval, J.-L.; Wittmer, C. R.; Gaut, L.; Duprez, D.; Egles, C.; Bedoui, F.; Schlatter, G.; Legallais, C. Poly(ε-Caprolactone)/Hydroxyapatite 3D Honeycomb Scaffolds for a Cellular Microenvironment Adapted to Maxillofacial Bone Reconstruction. *ACS Biomater. Sci. Eng.* **2018**, *4* (9), 3317–3326. https://doi.org/10.1021/acsbiomaterials.8b00521.

(9) Augustine, R.; Dalvi, Y. B.; Dan, P.; George, N.; Helle, D.; Varghese, R.; Thomas, S.; Menu, P.; Sandhyarani, N. Nanoceria Can Act as the Cues for Angiogenesis in Tissue-Engineering Scaffolds: Toward Next-Generation in Situ Tissue Engineering. *ACS Biomater. Sci. Eng.* **2018**, *4* (12), 4338–4353. https://doi.org/10.1021/acsbiomaterials.8b01102.

(10) Cipitria, A.; Skelton, A.; Dargaville, T. R.; Dalton, P. D.; Hutmacher, D. W. Design, Fabrication and Characterization of PCL Electrospun Scaffolds—a Review. *J. Mater. Chem.* **2011**, *21* (26), 9419. https://doi.org/10.1039/c0jm04502k.

(11) Li, D.; Xia, Y. Electrospinning of Nanofibers: Reinventing the Wheel? *Adv. Mater.* **2004**, *16* (14), 1151–1170. https://doi.org/10.1002/adma.200400719.

(12) Zong, H.; Xia, X.; Liang, Y.; Dai, S.; Alsaedi, A.; Hayat, T.; Kong, F.; Pan, J. H. Designing Function-Oriented Artificial Nanomaterials and Membranes via Electrospinning and Electrospraying Techniques. *Mater. Sci. Eng. C* **2018**, *92*, 1075–1091. https://doi.org/10.1016/j.msec.2017.11.007.

(13) Borah, R.; Ingavle, G. C.; Sandeman, S. R.; Kumar, A.; Mikhalovsky, S. V. Amine-Functionalized Electrically Conductive Core–Sheath MEH-PPV:PCL Electrospun Nanofibers for Enhanced Cell–Biomaterial Interactions. *ACS Biomater. Sci. Eng.* **2018**, *4* (9), 3327–3346. https://doi.org/10.1021/acsbiomaterials.8b00624.

(14) Bourdon, L.; Maurin, J.-C.; Gritsch, K.; Brioude, A.; Salles, V. Improvements in Resolution of Additive Manufacturing: Advances in Two-Photon Polymerization and Direct-Writing Electrospinning Techniques. *ACS Biomater. Sci. Eng.* **2018**, *4* (12), 3927–3938. https://doi.org/10.1021/acsbiomaterials.8b00810.

(15) Suwantong, O. Biomedical Applications of Electrospun Polycaprolactone Fiber Mats. *Polym. Adv. Technol.* **2016**, *27* (10), 1264–1273. https://doi.org/10.1002/pat.3876.

(16) Malikmammadov, E.; Tanir, T. E.; Kiziltay, A.; Hasirci, V.; Hasirci, N. PCL and PCL-Based Materials in Biomedical Applications. *J. Biomater. Sci. Polym. Ed.* **2018**, *29* (7–9), 863–893. https://doi.org/10.1080/09205063.2017.1394711.

(17) Ghosal, K.; Manakhov, A.; Zajíčková, L.; Thomas, S. Structural and Surface Compatibility Study of Modified Electrospun Poly(ε-Caprolactone) (PCL) Composites for Skin Tissue Engineering. *AAPS PharmSciTech* **2017**, *18* (1), 72–81. https://doi.org/10.1208/s12249-016-0500-8.

(18) Ko, Y.-M.; Choi, D.-Y.; Jung, S.-C.; Kim, B.-H. Characteristics of Plasma Treated Electrospun Polycaprolactone (PCL) Nanofiber Scaffold for Bone Tissue Engineering. *J. Nanosci. Nanotechnol.* **2015**, *15* (1), 192–195. https://doi.org/10.1166/jnn.2015.8372.

(19) Kudryavtseva, V.; Stankevich, K.; Kibler, E.; Golovkin, A.; Mishanin, A.; Bolbasov, E.; Choynzonov, E.; Tverdokhlebov, S. The Deposition of Thin Titanium-Nitrogen Coatings on the Surface of PCL-Based Scaffolds for Vascular Tissue Engineering. *Appl. Phys. Lett.* **2018**, *112* (15), 153705. https://doi.org/10.1063/1.5017580.

(20) Gautam, S.; Chou, C.-F.; Dinda, A. K.; Potdar, P. D.; Mishra, N. C. Surface Modification of Nanofibrous Polycaprolactone/Gelatin Composite Scaffold by Collagen Type I Grafting for Skin Tissue Engineering. *Mater. Sci. Eng. C* **2014**, *34*, 402–409. https://doi.org/10.1016/j.msec.2013.09.043.

(21) Ghosal, K.; Chandra, A.; G., P.; S., S.; Roy, S.; Agatemor, C.; Thomas, S.; Provaznik, I. Electrospinning over Solvent Casting: Tuning of Mechanical Properties of Membranes. *Sci. Rep.* **2018**, *8* (1), 5058. https://doi.org/10.1038/s41598-018-23378-3.

(22) Domingos, M.; Intranuovo, F.; Gloria, A.; Gristina, R.; Ambrosio, L.; Bártolo, P. J.; Favia, P. Improved Osteoblast Cell Affinity on Plasma-Modified 3-D Extruded PCL Scaffolds. *Acta Biomater.* **2013**, *9* (4), 5997–6005. https://doi.org/10.1016/j.actbio.2012.12.031.

(23) Goreninskii, S. I.; Bolbasov, E. N.; Sudarev, E. A.; Stankevich, K. S.; Anissimov, Y. G.; Golovkin, A. S.; Mishanin, A. I.; Viknianshchuk, A. N.; Filimonov, V. D.; Tverdokhlebov, S. I. Fabrication and Properties of l -Arginine-Doped PCL Electrospun Composite Scaffolds. *Mater. Lett.* **2018**, *214*, 64–67. https://doi.org/10.1016/j.matlet.2017.11.115.

(24) Bolbasov, E. N.; Maryin, P. V.; Stankevich, K. S.; Goreninskii, S. I.; Kudryavtseva, V. L.; Mishanin, A. I.; Golovkin, A. S.; Malashicheva, A. B.; Zhukov, Y. M.; Anissimov, Y. G.; Tverdokhlebov, S. I. Nitrogen-Doped Titanium Dioxide Thin Films Formation on the Surface of PLLA Electrospun Microfibers Scaffold by Reactive Magnetron Sputtering Method. *Plasma Chem. Plasma Process.* **2019**, *39* (2), 503–517. https://doi.org/10.1007/s11090-019-09956-x.

(25) Bolbasov, E. N.; Maryin, P. V.; Stankevich, K. S.; Kozelskaya, A. I.; Shesterikov, E. V.; Khodyrevskaya, Y. I.; Nasonova, M. V.; Shishkova, D. K.; Kudryavtseva, Y. A.; Anissimov, Y. G.; Tverdokhlebov, S. I. Surface Modification of Electrospun Poly-(l-Lactic) Acid Scaffolds by Reactive Magnetron Sputtering. *Colloids Surfaces B Biointerfaces* **2018**, *162*, 43–51. https://doi.org/10.1016/j.colsurfb.2017.11.028.

(26) Barbarash, L. S.; Bolbasov, E. N.; Antonova, L. V.; Matveeva, V. G.; Velikanova, E. A.; Shesterikov, E. V.; Anissimov, Y. G.; Tverdokhlebov, S. I. Surface Modification of Poly-ε-Caprolactone Electrospun Fibrous Scaffolds Using Plasma Discharge with Sputter Deposition of a Titanium Target. *Mater. Lett.* **2016**, *171*, 87–90. https://doi.org/10.1016/j.matlet.2016.02.062.

(27) Anderson, J. M.; Rodriguez, A.; Chang, D. T. Foreign Body Reaction to Biomaterials. *Semin. Immunol.* **2008**, *20* (2), 86–100. https://doi.org/10.1016/j.smim.2007.11.004.

(28) Vishwakarma, A.; Bhise, N. S.; Evangelista, M. B.; Rouwkema, J.; Dokmeci, M. R.; Ghaemmaghami, A. M.; Vrana, N. E.; Khademhosseini, A. Engineering Immunomodulatory Biomaterials To Tune the Inflammatory Response. *Trends Biotechnol.* **2016**, *34* (6), 470–482. https://doi.org/10.1016/j.tibtech.2016.03.009.

(29) Sridharan, R.; Cameron, A. R.; Kelly, D. J.; Kearney, C. J.; O'Brien, F. J. Biomaterial Based Modulation of Macrophage Polarization: A Review and Suggested Design Principles. *Mater. Today* **2015**, *18* (6), 313–325. https://doi.org/10.1016/j.mattod.2015.01.019.

(30) Kzhyshkowska, J.; Gudima, A.; Riabov, V.; Dollinger, C.; Lavalle, P.; Vrana, N. E. Macrophage Responses to Implants: Prospects for Personalized Medicine. *J. Leukoc. Biol.* **2015**, *98* (6), 953–962. https://doi.org/10.1189/jlb.5VMR0415-166R.

(31) Alvarez, M. M.; Liu, J. C.; Trujillo-de Santiago, G.; Cha, B.-H.; Vishwakarma, A.; Ghaemmaghami, A. M.; Khademhosseini, A. Delivery Strategies to Control Inflammatory Response: Modulating M1–M2 Polarization in Tissue Engineering Applications. *J. Control. Release* **2016**, *240*, 349–363. https://doi.org/10.1016/j.jconrel.2016.01.026.

(32) Hotchkiss, K. M.; Reddy, G. B.; Hyzy, S. L.; Schwartz, Z.; Boyan, B. D.; Olivares-Navarrete, R. Titanium Surface Characteristics, Including Topography and Wettability, Alter Macrophage Activation. *Acta Biomater.* **2016**, *31*, 425–434. https://doi.org/10.1016/j.actbio.2015.12.003.

(33) Lv, L.; Xie, Y.; Li, K.; Hu, T.; Lu, X.; Cao, Y.; Zheng, X. Unveiling the Mechanism of Surface Hydrophilicity-Modulated Macrophage Polarization. *Adv. Healthc. Mater.* **2018**, *7* (19), 1800675. https://doi.org/10.1002/adhm.201800675.

(34) Zhao, F.; Wang, C.; Yang, Q.; Han, S.; Hu, Q.; Fu, Z. Titanium Dioxide Nanoparticle Stimulating Pro-Inflammatory Responses in Vitro and in Vivo for Inhibited Cancer Metastasis. *Life Sci.* **2018**, *202*, 44–51. https://doi.org/10.1016/j.lfs.2018.03.058.

(35) Chen, Q.; Wang, N.; Zhu, M.; Lu, J.; Zhong, H.; Xue, X.; Guo, S.; Li, M.; Wei, X.; Tao, Y.; Yin, H. TiO 2 Nanoparticles Cause Mitochondrial Dysfunction, Activate Inflammatory Responses, and Attenuate Phagocytosis in Macrophages: A Proteomic and Metabolomic Insight. *Redox Biol.* **2018**, *15*, 266–276. https://doi.org/10.1016/j.redox.2017.12.011.

(36) Bolbasov, E. N.; Antonova, L. V.; Stankevich, K. S.; Ashrafov, A.; Matveeva, V. G.; Velikanova, E. A.; Khodyrevskaya, Y. I.; Kudryavtseva, Y. A.; Anissimov, Y. G.; Tverdokhlebov, S. I.; Barbarash, L. S. The Use of Magnetron Sputtering for the Deposition of Thin Titanium Coatings on the Surface of Bioresorbable Electrospun Fibrous Scaffolds for Vascular Tissue Engineering: A Pilot Study. *Appl. Surf. Sci.* **2017**, *398*, 63–72. https://doi.org/10.1016/j.apsusc.2016.12.033.

(37) Frisch, M. J.; Trucks, G. W.; Schlegel, H. B.; Scuseria, G. E.; Robb, M. A.; Cheeseman, J. R.; Scalmani, G.; Barone, V.; Petersson, G. A.; Nakatsuji, H.; Li, X.; Caricato, M.; Marenich, A. V.; Bloino, J.; Janesko, B. G.; Gomperts, R.; Mennucci, B.; Hratchian, H. P.; Ortiz, J. V.; Izmaylov, A. F.; Sonnenberg, J. L.; Williams; Ding, F.; Lipparini, F.; Egidi, F.; Goings, J.; Peng, B.; Petrone, A.; Henderson, T.; Ranasinghe, D.; Zakrzewski, V. G.; Gao, J.; Rega, N.; Zheng, G.; Liang, W.; Hada, M.; Ehara, M.; Toyota, K.; Fukuda, R.; Hasegawa, J.; Ishida, M.; Nakajima, T.; Honda, Y.; Kitao, O.; Nakai, H.; Vreven, T.; Throssell, K.; Montgomery Jr., J. A.; Peralta, J. E.; Ogliaro, F.; Bearpark, M. J.; Heyd, J. J.; Brothers, E. N.; Kudin, K. N.; Staroverov, V. N.; Keith, T. A.; Kobayashi, R.; Normand, J.; Raghavachari, K.; Rendell, A. P.; Burant, J. C.; Iyengar, S. S.; Tomasi, J.; Cossi, M.; Millam, J. M.; Klene, M.; Adamo, C.; Cammi, R.; Ochterski, J. W.; Martin, R. L.; Morokuma, K.; Farkas, O.; Foresman, J. B.; Fox, D. J. G16_C01.

(38) Becke, A. D. Density-functional Thermochemistry. III. The Role of Exact Exchange. *J. Chem. Phys.* **1993**, *98* (7), 5648–5652. https://doi.org/10.1063/1.464913.

(39) Demir, P.; Akman, F. Molecular Structure, Spectroscopic Characterization, HOMO and LUMO Analysis of PU and PCL Grafted onto PEMA-Co-PHEMA with DFT Quantum Chemical Calculations. *J. Mol. Struct.* **2017**, *1134*, 404–415.

https://doi.org/10.1016/j.molstruc.2016.12.101.

(40) Popova, A.; Kzhyshkowska, J.; Nurgazieva, D.; Goerdt, S.; Gratchev, A. Pro- and Anti-Inflammatory Control of M-CSF-Mediated Macrophage Differentiation. *Immunobiology* **2011**, *216* (1–2), 164–172. https://doi.org/10.1016/j.imbio.2010.06.003.

(41) Neuhäuser, M.; Bärwulf, S.; Hilgers, H.; Lugscheider, E.; Riester, M. Optical Emission Spectroscopy Studies of Titanium Nitride Sputtering on Thermoplastic Polymers. *Surf. Coatings Technol.* **1999**, *116–119*, 981–985. https://doi.org/10.1016/S0257-8972(99)00214-5.

(42) Riester, M.; Bärwulf, S.; Lugscheider, E.; Hilgers, H. Morphology of Sputtered Titanium Nitride Thin Films on Thermoplastic Polymers. *Surf. Coatings Technol.* **1999**, *116–119*, 1001–1005. https://doi.org/10.1016/S0257-8972(99)00188-7.

(43) Miller, A.; Carchman, R.; Long, R.; Denslow, S. A. La Crosse Viral Infection in Hospitalized Pediatric Patients in Western North Carolina. *Hosp. Pediatr.* **2012**, *2* (4), 235–242. https://doi.org/10.1542/hpeds.2012-0022.

(44) Kudryavtseva, V.; Stankevich, K.; Kibler, E.; Golovkin, A.; Mishanin, A.; Bolbasov, E.; Choynzonov, E.; Tverdokhlebov, S. The Deposition of Thin Titanium-Nitrogen Coatings on the Surface of PCL-Based Scaffolds for Vascular Tissue Engineering. *Appl. Phys. Lett.* **2018**, *112* (15). https://doi.org/10.1063/1.5017580.

(45) O'Connell, C.; Sherlock, R.; Ball, M. D.; Aszalós-Kiss, B.; Prendergast, U.; Glynn, T. J. Investigation of the Hydrophobic Recovery of Various Polymeric Biomaterials after 172nm UV Treatment Using Contact Angle, Surface Free Energy and XPS Measurements. *Appl. Surf. Sci.* **2009**, *255* (8), 4405–4413. https://doi.org/10.1016/j.apsusc.2008.11.034.

(46) Intranuovo, F.; Gristina, R.; Brun, F.; Mohammadi, S.; Ceccone, G.; Sardella, E.; Rossi, F.; Tromba, G.; Favia, P. Plasma Modification of PCL Porous Scaffolds Fabricated by Solvent-Casting/Particulate-Leaching for Tissue Engineering. *Plasma Process. Polym.* **2014**, *11* (2), 184–195. https://doi.org/10.1002/ppap.201300149.

(47) Tawil, N.; Sacher, E.; Boulais, E.; Mandeville, R.; Meunier, M. X-Ray Photoelectron Spectroscopic and Transmission Electron Microscopic Characterizations of Bacteriophage–Nanoparticle Complexes for Pathogen Detection. *J. Phys. Chem. C*

2013, *117* (40), 20656–20665. https://doi.org/10.1021/jp406148h.

(48) Suska, F.; Gretzer, C.; Esposito, M.; Tengvall, P.; Thomsen, P. Monocyte Viability on Titanium and Copper Coated Titanium. *Biomaterials* **2005**, *26* (30), 5942–5950. https://doi.org/10.1016/j.biomaterials.2005.03.017.

(49) Xiang, P.; Wang, S.-S.; He, M.; Han, Y.-H.; Zhou, Z.-H.; Chen, D.-L.; Li, M.; Ma, L. Q. The in Vitro and in Vivo Biocompatibility Evaluation of Electrospun Recombinant Spider Silk Protein/PCL/Gelatin for Small Caliber Vascular Tissue Engineering Scaffolds. *Colloids Surfaces B Biointerfaces* **2018**, *163*, 19–28. https://doi.org/10.1016/j.colsurfb.2017.12.020.

(50) Wang, Z.; Cui, Y.; Wang, J.; Yang, X.; Wu, Y.; Wang, K.; Gao, X.; Li, D.; Li, Y.; Zheng, X.-L.; Zhu, Y.; Kong, D.; Zhao, Q. The Effect of Thick Fibers and Large Pores of Electrospun Poly(ε-Caprolactone) Vascular Grafts on Macrophage Polarization and Arterial Regeneration. *Biomaterials* **2014**, *35* (22), 5700–5710. https://doi.org/10.1016/j.biomaterials.2014.03.078.

(51) Wang, Z.; Cui, Y.; Wang, J.; Yang, X.; Wu, Y.; Wang, K.; Gao, X.; Li, D.; Li, Y.; Zheng, X.-L.; Zhu, Y.; Kong, D.; Zhao, Q. The Effect of Thick Fibers and Large Pores of Electrospun Poly(ε-Caprolactone) Vascular Grafts on Macrophage Polarization and Arterial Regeneration. *Biomaterials* **2014**, *35* (22), 5700–5710. https://doi.org/10.1016/j.biomaterials.2014.03.078.

For Table of Contents Use Only

Modification of PCL scaffolds by reactive magnetron sputtering: a possibility for modulating macrophage responses

Ksenia S. Stankevich[1,2], Valeriya L. Kudryavtseva[3,1], Evgeny N. Bolbasov[1,4], Evgeny V. Shesterikov[4,5], Irina V. Larionova[6,7], Yelena G. Shapovalova[6], Liubov V. Domracheva[6], Apollinariya A. Volokhova[1,6], Irina A. Kurzina[6], Yuri M. Zhukov[8], Anna B. Malashicheva[9,10], Julia G. Kzhyshkowska[6,10], Sergei I. Tverdokhlebov[1]

1. *National Research Tomsk Polytechnic University, 30 Lenin Avenue, Tomsk, 634050, Russian Federation.*
2. *Montana State University, Culbertson Hall 100, Bozeman, Montana, USA.*
3. *Queen Mary University of London, Mile End Rd, Bethnal Green, London E1 4NS United Kingdom.*
4. *V.E. Zuev Institute of Atmospheric Optics SB RAS, 1 Academician Zuev square Tomsk, 634055, Russian Federation.*
5. *Tomsk State University of Control Systems and Radioelectronics, 40 Lenin Avenue Tomsk, 634050, Russian Federation.*
6. *Tomsk State University, 36 Lenin Avenue Tomsk, 634050, Russian Federation.*
7. *Cancer Research Institute, Tomsk National Research Medical Center, Russian Academy of Sciences, 9 Kooperativnii pereulok, Tomsk, 634050, Russian Federation.*
8. *Saint-Petersburg State University, 11/2 Lieutenant Schmidt emb., St. Petersburg, 199034 Russian Federation.*
9. *ITMO University, Institute of translational Medicine, 49 Kronverksky prospekt, Saint Petersburg, 197101, Russian Federation.*
10. *Federal Almazov Medical Research Centre, 2 Akkuratova street, St. Petersburg, 19734, Russian Federation.*